Supplementary Materials:
Bifurcation of time crystals in driven and dissipative Rydberg atomic gas

Bang Liu[1,2], Li-Hua Zhang[1,2], Yu Ma[1,2], Qi-Feng Wang[1,2], Tian-Yu Han[1,2], Jun Zhang[1,2], Zheng-Yuan Zhang[1,2], Shi-Yao Shao[1,2], Qing Li[1,2], Han-Chao Chen[1,2], Guang-Can Guo[1,2], Dong-Sheng Ding[1,2,†], and Bao-Sen Shi[1,2]

[1] *Key Laboratory of Quantum Information, University of Science and Technology of China; Hefei, Anhui 230026, China. and*
[2] *Synergetic Innovation Center of Quantum Information and Quantum Physics, University of Science and Technology of China; Hefei, Anhui 230026, China.*

SUPPLEMENTARY NOTE 1: DETAILS OF THE EXPERIMENTAL SETUP

Supplementary Fig. 1(b) shows the measured EIT spectrum under the external RF field driving conditions, in which the frequency of the RF field was set at $\omega = 2\pi\times 8.1$ MHz. Supplementary Fig. 1(c) and (d) represent the oscillated transmission and the Fourier transformation spectrum, respectively. The oscillated behavior was caused by the population of Rydberg atoms oscillating between two energy states with a specific period, creating a temporal order [with a frequency of $\sim 2\pi\times 19$ kHz], and displaying the characteristics of a continuous dissipative time crystal.

In the quench dynamics measurement [see Supplementary Fig. 1(e)], we measured the oscillated transmission by switching the RF field on. By selecting data points within the interval from $t_1 \sim t_2$, as depicted in Supplementary Fig. 1(e), we obtained the real and imaginary parts of the amplitude of the dominant peak in the Fourier spectrum. In this process, we used 300 data points acquired from multiple experimental trials to construct the plots shown in Fig. 1(e) and Fig. 1(f).

When the RF field is switched on, the system initially carries out an evolution that is not completely disordered but with the phase $\pi/2 \sim 3\pi/2$ missing, which means that the probe transmission oscillates within the phase distribution from $-\pi/2 \sim \pi/2$ at a small $t_1 = 0.05$ ms, as shown in Supplementary Fig. 1(f). After an additional period of time, the system is completely out of order, as shown in Supplementary Fig. 1(g)-(i), and the oscillation then becomes completely random when $t_1 = 3.93$ ms. This occurs because the system is inclined to remain in a stationary phase at a small t_1, whereas it exhibits persistent oscillations with random phases at larger t_1 values, thus revealing the essence of spontaneous breaking of the time translation symmetry.

SUPPLEMENTARY NOTE 2: COMPARISON OF DIFFERENT PROBE INTENSITIES

The oscillated behavior during probe transmission indicates the existence of a time crystal, and this is closely related to the long-range interactions occurring between the Rydberg atoms. In the experiments, we observed evidence of this behavior by changing the population of the excited Rydberg atoms. Using the same measurement method that was used in the work in the main text, we obtained the Fourier spectrum of the system response, as shown in Supplementary Fig. 2, by scanning the voltage from $U = 0$ V to $U = 5$ V at various probe field intensities. Therefore, we changed the probe intensities to excite different numbers of Rydberg atoms, and obtained different phase maps for the Fourier spectrum. When the probe intensity was set at 64 μW, the Fourier spectrum showed a series of peaks, as indicated in Supplementary Fig. 2(a), which corresponded to distinct time crystal phases. In addition, we observed the time crystal phase of splitting and transitioning, which is caused by scanning of the voltage U with an opposite direction, similar to that in Fig. 4 and Fig. 5 as described in the main text. Supplementary Figure 2(b) shows the Fourier spectrum at $U = 3$ V, where several peaks are present in the spectrum.

However, when the probe intensity decreases to 3.5 μW, the EIT spectrum still exists, but the oscillated behavior observed in probe transmission disappears. In addition, the Fourier spectrum of the system shows irregular noise, as illustrated in Supplementary Fig. 2(c), without any peaks [see the example in Supplementary Fig. 2(d) at $U =$ 3 V]. In this scenario, the number of Rydberg atoms is small because of the weak probing light, which results in weaker interactions between the Rydberg atoms. Furthermore, the oscillated behavior of the system disappears and the system then enters the normal phase from the time crystal phase. This suggests that the long-range interaction is responsible for the emergence of the time crystal.

---

† dds@ustc.edu.cn

SUPPLEMENTARY NOTE 3: FLOQUET THEORY OF THE COUPLING OF RYDBERG ATOMS AND THE RF FIELD

To describe the coupling between the RF field and the Rydberg atoms and to explain the reason for generation of the RF sidebands, we introduce the Floquet theory. In the Floquet treatment, the RF field is viewed as a periodic driving signal, and the Hamiltonian of the system is written as follows:

$$H(t) = H_0 + e\boldsymbol{R} \cdot \boldsymbol{E}\cos(\omega \mathrm{t}) \tag{1}$$

where H_0 is the Hamiltonian of the atomic system in the absence of the field, $e\boldsymbol{R}$ is the dipole moment of Rydberg atom and $\boldsymbol{E}$ is the intensity of the RF field. We consider the larger intensity of the rf-field, the driving can be described by the Floquet theory [1], the wave functions of a time-periodic Hamiltonian system can be written in the following form:

$$\Psi_\nu(t) = e^{-iW_\nu t/\hbar}\psi_\nu(t) \tag{2}$$

This wave function can be expanded using the standard basis states $|k\rangle$:

$$\Psi_\nu(t) = e^{-iW_\nu t/\hbar}\sum_k \sum_{m=-\infty}^{\infty} \tilde{C}_{\nu,k,m} e^{-im\omega t}|k\rangle \tag{3}$$

where W_ν are the Floquet quasi-energies determined by finding the eigenvalues of the time-evolution operator, the integer m represents the order of the sidebands, $\tilde{C}_{\nu,k,m}$ is the Fourier expansion coefficient and $|k\rangle = |n, l, j, m_j\rangle$ are the standard basis states in the absence of external fields. The energies of the different sidebands are given by

$$\hbar\omega_m = W_\nu + m\hbar\omega \tag{4}$$

Under the RF electric field driving condition, the Rydberg energy levels form a series of equally spaced Floquet energy levels with the energy level spacing $\hbar\omega$. To model the oscillated spectrum of time crystal, we only consider the ±1-order sidebands, as shown in Fig. 1(a). Periodic driving of the RF field leads to sidebands of the Rydberg states. In the extended Floquet Hilbert space, we can obtain the time independent effective Hamiltonian of the system [2].

SUPPLEMENTARY NOTE 4: NUMERICAL SIMULATION RESULTS

We therefore obtained the population of the Rydberg states ρ_{RR}, $\rho_{\mathrm{R_1R_1}}$, and $\rho_{\mathrm{R_2R_2}}$ versus time, as shown in Supplementary Fig. 3. Supplementary Figure 3(a) shows the results obtained with no interaction, where the system will reach a steady state after a specified time [typically in the range from $\gamma t = 0$ to $\gamma t = 100$]. The Fourier spectrum of the data points from $\gamma t = 100 \sim 200$ in Supplementary Fig. 3(a) is shown in Supplementary Fig. 3(b). Supplementary Figure 3(e) shows the results obtained with interaction $\xi = -16$, in which the system achieves long-time oscillation, thus meaning that it enters a limit cycle phase. The Fourier spectrum of the data points from $\gamma t = 100 \sim 200$ shown in Supplementary Fig. 3(b) is given in Supplementary Fig. 3(f). There are visible peaks in the amplitude in Supplementary Fig. 3(f).

In addition, we plot the dynamical evolution with the parameters $\rho_{R_1R_1}[t]$, $\rho_{gR}[t]$, $\rho_{RR}[t]$, the atoms end at an identical fixed point in phase space (Supplementary Fig. 3(c)) with no interaction, while display nontrivial oscillations (Supplementary Fig. 3(g)) with interaction $\xi = -16$. These processes are irrelevant to initial states, which are shown by the red and black lines in Supplementary Fig. 3(c) and Supplementary Fig. 3(g). By tuning the parameters, we can obtain the long-time oscillations with distinct frequencies of f_0 and $f_0/2$ as shown in Supplementary Fig. 3(i,j), corresponding to multiple time crystals. And the trajectories of the system evolution are intertwined in phase space, as shown in Supplementary Fig. 3(k,l). In the numerical results, although several parameters affect the appearance of the second peak, we find that the Rabi frequency Ω plays a dominant role. By varying the intensity of the Rabi frequency Ω while keeping the other parameters constant, we can observe the second peak appearing gradually. This is because the driving strength increases, leading to a higher number of excited Rydberg atoms. The interaction between these atoms disrupts the synchronization of the system. The stability of the phase space trajectory of the system is altered, causing the orbits of the limit cycle to diverge. Eventually the system response exhibits a new period and the results are shown in Supplementary Fig. 3(d,h,l). The period doubling bifurcation effect is an important route to chaos [3].

In addition, we plot Fourier spectrum of the population ρ_{RR} versus ξ, δ, and $\Omega_{1/2}$, as shown in Supplementary Fig. 4(a-c). In Supplementary Fig. 4(a), there is a linear regime in which the oscillation frequency is proportional to the interaction strength around ξ=-14 [regime A in Supplementary Fig. 4(a)], revealing that the interaction plays a vital role in generating oscillations. In both of Supplementary Fig. 4(b) and Supplementary Fig. 4(c), the time crystal can be found in a range of δ and $\Omega_{1/2}$, in which δ and $\Omega_{1/2}$ are related to the parameters w and U in experiment. In Supplementary Fig. 4(b), with a increase of δ, the frequency of time crystal increases and the amplitude decreases, which is consistent with experimental observations in Supplementary Fig. 2(d) by changing ω.

SUPPLEMENTARY REFERENCE

[1] D. A. Anderson, S. A. Miller, G. Raithel, J. A. Gordon, M. L. Butler, and C. L. Holloway, Optical measurements of strong microwave fields with Rydberg atoms in a vapor cell, Phys. Rev. Appl. **5**, 034003 (2016).

[2] A. Eckardt and E. Anisimovas, High-frequency approximation for periodically driven quantum systems from a floquet-space perspective, New Journal of Physics **17**, 093039 (2015).

[3] S. H. Strogatz, *Nonlinear dynamics and chaos: with applications to physics, biology, chemistry, and engineering* (CRC press, 2018).

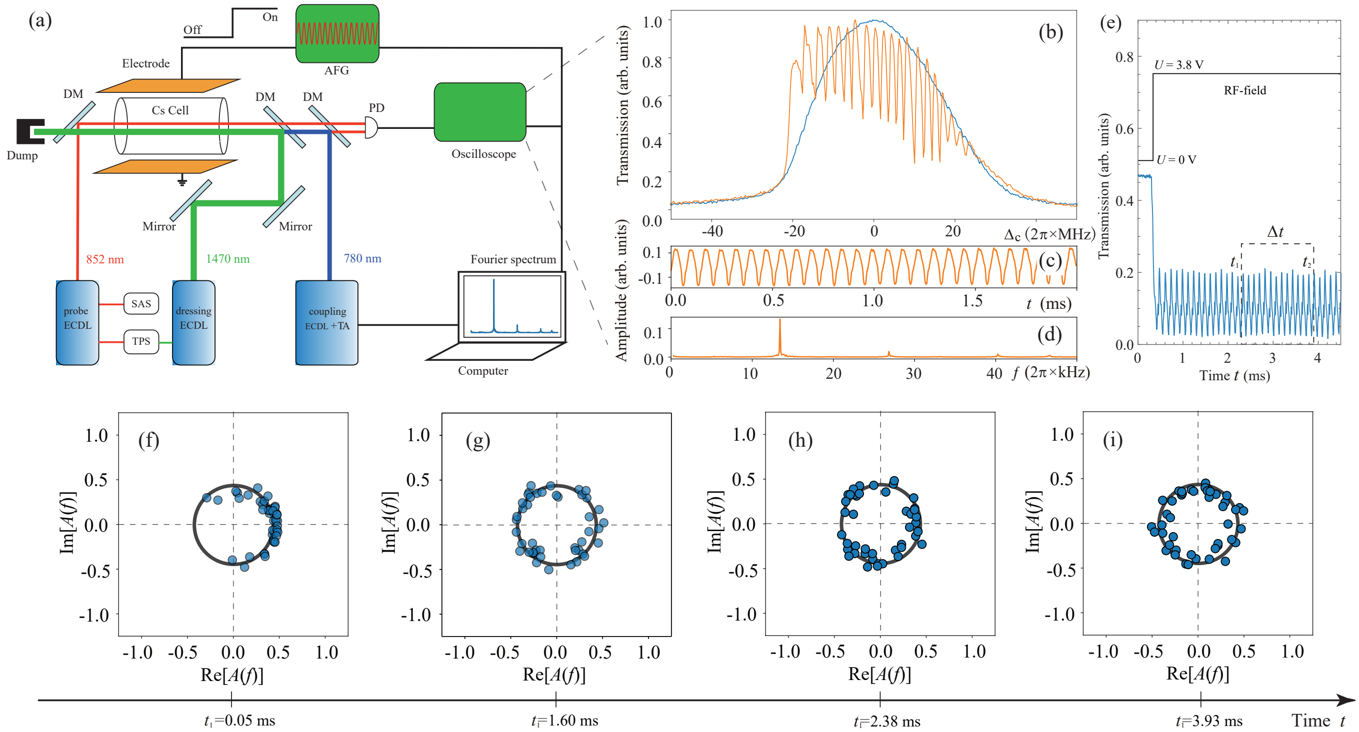

Supplementary Figure 1: **Details of experimental setup and probe transmission oscillations.** (a) Experimental setup. ECDL: external-cavity diode laser. PD: photoelectric detector. TA: tapered amplifier. AFG: arbitrary function generator. SAS: saturated absorption spectrum. DM: dichroic mirror. The dump is used to collect the optical beam. The computer is used to analyze the Fourier spectrum and visualize the data. (b) The EIT spectra with (orange) and without (blue) the external RF field. (c) shows the oscillated EIT transmission in the time domain, and (d) represents the Fourier spectrum of the time crystal. The first peak characterizes the frequency of the time crystal. (e) Quench dynamics of the probe transmission caused by switching of the RF field. (f)-(i) Measured distribution of the Fourier amplitudes with the dominant peak on the complex plane realized by selecting different starting times of $t_1 = 0.05$ ms (f), 1.60 ms (g), 2.38 ms (h), and 3.93 ms (i) within the time interval $\Delta t = 0.775$ ms.

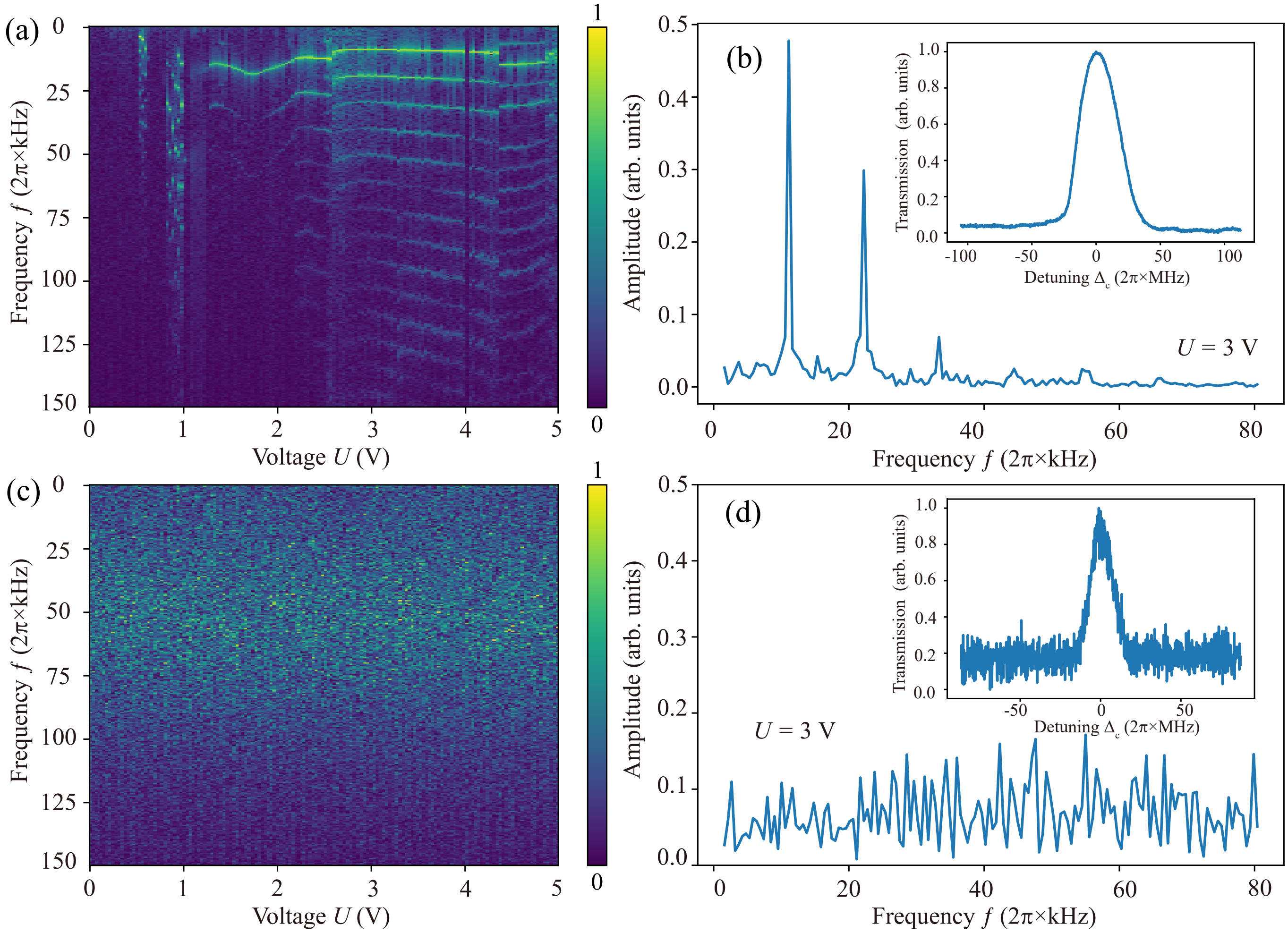

Supplementary Figure 2: **Normalized Fourier spectra with different probe intensities.** Fourier map of a section of the voltage U range from 0 V to 5 V with a probe intensity of 64 μW in (a) and of 3.5 μW in (c). In (a), distinct peaks can be found, whereas only irregular noise is found in panel (c). The color bar ranging from 0 to 1 represents the Fourier transform intensity. (b) and (d) show the corresponding Fourier spectra at $U = 3$ V. The insets are the EIT spectra with a probe intensity of 64 μW in (b) and of 3.5 μW in (d).

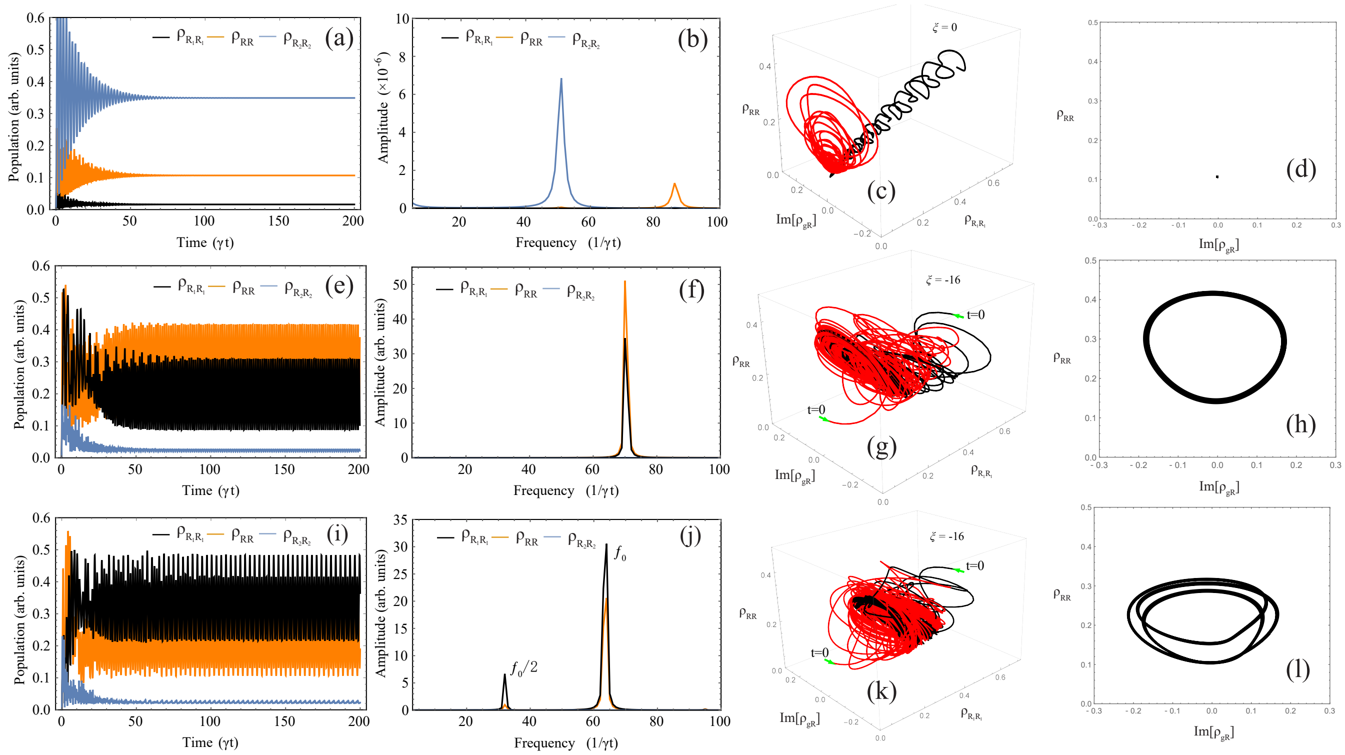

Supplementary Figure 3: **Oscillations in phase space.** Calculated population of the Rydberg states ρ_{RR}, $\rho_{\mathrm{R_1R_1}}$, and $\rho_{\mathrm{R_2R_2}}$ versus time with no interaction $\xi = 0$ (a) and with interaction (e). In (b) and (f), the parameters Ω =3.5, $\Omega_{1/2} = 3$, $\gamma = 0.1$, $\delta = 7$, and $\Delta = -5$ are selected. (b), (f) and (j) show the corresponding Fourier spectra of the data points from $\gamma t = 100 \sim 200$ in (a), (e) and (i), respectively. From these results, we find that the peak amplitude in (b) is much lower than that in (f). (i) and (j) are calculated population and Fourier spectrum for time crystals with distinct frequencies of f_0 and $f_0/2$. In (j), the parameters Ω =2.3, $\Omega_{1/2} = 3.3$, $\gamma = 0.1$, $\delta = 7$, and $\Delta = -5.05$ are selected. Evolution of systems in phase space of ρ_{RR}, $\mathrm{Im}[\rho_{\mathrm{gR}}]$, and $\rho_{\mathrm{R_1R_1}}$ with no interaction $\xi = 0$ for (c), and with interaction $\xi = -16$ for (g) and (k). (d), (h), and (l) are the corresponding trajectories in phase space of ρ_{RR} and $\mathrm{Im}[\rho_{\mathrm{gR}}]$ with $\gamma t = 150 \sim 100$. The initial conditions in these cases are $\rho_{R_1R_1} = 0.0$, $\rho_{gR} = 0.1$, ρ_{RR} = 0.15 for red line and $\rho_{R_1R_1} = 0.7$, $\rho_{gR} = 0.2$, $\rho_{RR} = 0.3$ for black line. In (g) and (k), the green arrow represents the initial point at t=0.

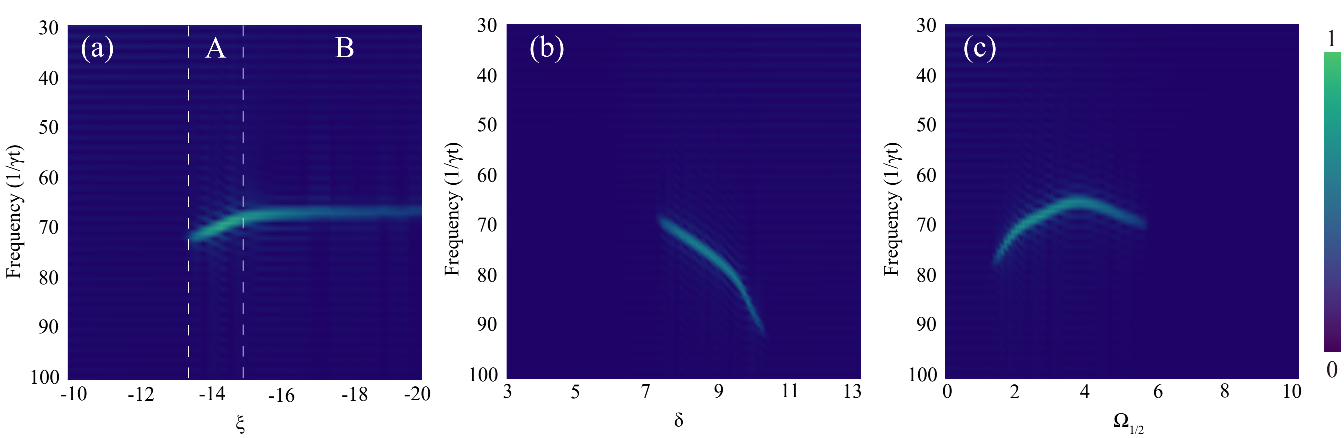

Supplementary Figure 4: **Fourier spectrum VS ξ, δ, and $\Omega_{1/2}$.** Simulated Fourier spectrum of the population ρ_{RR} versus ξ (a), δ (b), and $\Omega_{1/2}$ (c). In (a), there are two regimes, the frequency is proportional to ξ in regime A and constant with ξ in regime B. The conditions used here are Δ = -5, γ = 0.73, Ω = 3.5, $\Omega_{1/2}$ = 3, δ =7 for (a); Δ = -5, ξ = -16, γ = 0.73, Ω = 3.5, $\Omega_{1/2}$ = 3 for (b); Δ = -5, ξ = -16, γ = 0.73, Ω = 3, δ =7 for (c).